

Research paper

Percolation in random sequential adsorption of lattice animals on a three-dimensional cubic lattice

D. Stojiljković^{a,*}, J.R. Šćepanović^a, Z.M. Jakšić^a, Lj. Budinski-Petković^b, S.B. Vrhovac^a^a Institute of Physics Belgrade, University of Belgrade, Pregrevica 118, Belgrade 11080, Serbia^b Faculty of Technical Sciences, University of Novi Sad, Trg D. Obradovića 6, Novi Sad 21000, Serbia

ARTICLE INFO

Keywords:

Random sequential adsorption

Three-dimensional (3D) lattice

Lattice animals

Percolations

ABSTRACT

Percolation properties of the Random Sequential Adsorption (RSA) of objects of various shapes on simple three-dimensional (3D) cubic lattice are studied numerically by means of Monte Carlo simulations. Depositing objects are “lattice animals”, made of a certain number of nearest neighbor sites on a lattice. The aim of this work is to investigate the impact of the geometrical properties of the shapes on the values of percolation threshold θ_p^* . We analyzed all lattice animals of size $n \leq 5$.

Thanks to an extensive database of studied objects, we found that the number of nearest neighbors N_1 and the radius of gyration R_g of the objects are correlated with the values of percolation threshold θ_p^* . For lattice animals of the same size, the percolation threshold θ_p^* decreases with an increase in the number of the object's nearest neighbors N_1 . If objects of the same size n have the same number of nearest neighbors N_1 , their percolation threshold θ_p^* decreases with an increase in the radius of gyration R_g .

1. Introduction

A connected subgraph of a lattice is called a lattice animal. It can also be viewed as a finite set of lattice sites connected by a network of nearest neighbor bonds. In mathematics, and combinatorics in particular, terms polyominoes and polycubes are frequently used. A polyomino of size n is an edge-connected set of n squares on the square lattice \mathcal{Z}^2 (the set of integers is denoted by \mathcal{Z}). A polycube of size n is a face-connected set of n cubes in the cubic lattice \mathcal{Z}^3 . Because the square (cubic) lattice is self-dual, polyominoes (polycubes) are equivalent to lattice animals on the dual lattice.

Depending on the problem to be solved, *fixed* and *free* animals are distinguished. Fixed animals are considered distinct if they have different shapes or orientations. Free animals, on the other hand, are distinguished only by shape, not by orientation. In the mathematical literature, fixed polycubes are most discussed in the context of simple combinatorial problem — enumeration. Enumeration deals with determining the number of polycubes corresponding to a certain parameter, usually their size or perimeter [1]. It is very interesting that to this day there is no known analytic formula for calculation of the number of fixed d -dimensional polycubes of size n , $A_d(n)$, $d > 1$. The only known methods for computing $A_d(n)$ are based on explicitly or implicitly enumerating all the polyominoes or polycubes using various numerical algorithms [1–4]. Furthermore, the enumeration of lattice animals has traditionally served as a benchmark for computer performance and algorithm design [5–7].

* Corresponding author.

E-mail address: danica@ipb.ac.rs (D. Stojiljković).<https://doi.org/10.1016/j.cjph.2024.06.015>

Received 19 April 2024; Received in revised form 5 June 2024; Accepted 14 June 2024

Available online 18 June 2024

0577-9073/© 2024 The Physical Society of the Republic of China (Taiwan). Published by Elsevier B.V. All rights are reserved, including those for text and data mining, AI training, and similar technologies.

Extensive studies of lattice animals can also be found in statistical-physics literature, where fixed polycubes are usually referred to as strongly embedded lattice animals. Lattice animals play an important role in computing the mean cluster density in percolation processes [7,8]. Series expansions for the percolation probability or the average cluster size can be obtained as weighted sums over the number of lattice animals $g_{n,p}$, enumerated according to their size n and perimeter p [9]. Lattice animals have also been suggested as a model of branched polymers with excluded volume [10,11].

Recently, we have carried out extensive numerical simulations of random deposition of large collections of lattice animals and their binary mixtures on three-dimensional (3D) cubic lattices [12,13]. Random sequential adsorption (RSA) is a process in which particles of different shapes and sizes are constantly trying to attach themselves to randomly chosen places on the n -dimensional substrate [14]. If the incoming particle does not overlap any previously attached particles, it binds irreversibly. A quantity of central interest is the fraction of the substrate occupied by the deposited objects, $\theta(t)$, at time t . Because of the blocking effect by the already deposited particles, the limiting value θ_J is less than the close packing [15–17]. Due to the absence of relaxation, the formation of the limiting jammed state is governed by the infinite memory correlation effects.

In Refs. [12,13], we have found that the number of different orientations that lattice animals can take when placed on a cubic lattice exerts a decisive influence on the adsorption kinetics near the jamming limit θ_J . The results also suggested absence of correlation between the number of possible orientations of the object and the corresponding values of the jamming density θ_J . Depending on the local geometry of the objects making the mixture, the jamming coverage of a mixture θ_J^{mix} can be either greater than both single-component jamming coverages or can be in between these values. The first case is the most common, while in the second case, the jamming density of the mixture is very close to the higher jamming density for the pure component shapes.

During the RSA process, the number of deposited objects on the substrate increases so that they form clusters. A cluster is a group of occupied sites, so each site has at least one occupied nearest-neighbor site. Percolation assumes the existence of a large cluster that extends from one side to the opposite one of the system. In other words, percolation theory is based on finding the minimum coverage fraction for which a complete path of adjacent sites crossing the entire system becomes possible. This value of the fraction of the total area is named the effective percolation threshold θ_p . This transition is a geometrical phase transition where the critical concentration θ_p separates a phase of finite clusters from a phase where an infinite cluster is present. Forming long-range connectivity in disordered systems is important in many physical, chemical, and even sociological systems [18–20]. The percolation problem attracts considerable interest due to its applications in numerous practical issues, such as conductivity in composite materials, flow through porous media, polymerization, and behavior of scale-free random networks [21–26,26–33].

Numerous research papers have been published on percolations in three dimensions, which include some findings for more complex systems [34–38]. The study of irreversible deposition and percolation properties on 3D cubic lattices has mostly been focused on k -mers [39–41] and $k \times k \times l$ ($l = 1, k$) cubic objects [42,43]. Tarasevich and Cherkasova [39] have examined the percolation and jamming properties of dimers on simple 3D cubic lattices. In [41], the research of Tarasevich and Cherkasova has been extended to larger k -mers ($2 \leq k \leq 64$) to determine the relation between the jamming coverage and the size of the deposited k -mers for simple cubic lattices. The study has revealed that the ratio between the percolation threshold and the jamming coverage exhibits a nonuniversal behavior, decreasing to zero with an increase in k . These findings suggest that the percolation phase transition occurs for all values of k .

In the present study the percolation properties are analyzed for various shapes formed by connected sites on a 3D lattice. All lattice animals of size $n = 1 - 5$ (41 different shapes) are studied. Object size is the number n of nodes that a lattice animal covers on the grid. The number of examined lattice animals represents a good basis for studying the impact of the geometrical properties of the shapes on the jamming coverage θ_J and on the values of percolation threshold θ_p^* . Here, the relationship between the values of the percolation threshold θ_p^* of objects and the number of first neighbors N_1 and the gyration radius R_g of objects has been thoroughly analyzed. Random deposition of lattice animals on 3D lattices is a complex problem and it is difficult to develop even a qualitative understanding of the effects of shape on the packing density and percolation properties.

The paper is organized as follows. Section 2 describes the model and the details of the simulations. The percolation properties of lattice animals are analyzed in Section 3. Finally, Section 4 contains some additional comments.

2. Definition of the model and the simulation method

We are focusing solely on the free lattice animals on a simple cubic lattice (the term “free” is omitted in the following text). Table 1 shows all polycubes of size $n = 1, 2, 3$, and 4. Polycubes of size $n = 1, 2, 3$ are planar with a maximum of twelve different orientations (object V3). There are eight tetracubes (fourth-order polycubes), of which five are planar [44]. Polycubes are usually counted with mirror pairs (so-called chiral twins) distinguished, as would be natural for the cubical case in ordinary space. For example, a tetracube A4 and its mirror image B4 are considered distinct because there is no rigid motion that transforms one onto the other.

All polycubes of size $n = 5$ (pentacubes) are shown in Table 2. There are 29 distinct three-dimensional pentacubes [44]. As it can be seen, twelve pentacubes are flat and correspond to solid *pentominoes*. Among the nonplanar pentacubes, there are five that have at least one plane of symmetry (A5, L35, Q5, T15, T25) and each of them is its own mirror image. The remaining twelve nonplanar pentacubes form six chiral pairs: {J15, L15}, {J25, L25}, {J45, L45}, {N15, S15}, {N25, S25}, {V15, V25}. For two flats (I5, X5) of the 29 pentacubes, there are only three possible orientations. Ten pentacubes have twelve orientations and each of the remaining 17 pentacubes has 24 orientations.

As stated in Section 1, the structure of a polycube can be represented by means of a lattice animal that has a vertex for each cube and an edge for each two cubes that share a square. Several examples of lattice animals that are equivalent to corresponding

Table 1
All polycubes (x) of size $n = 1, 2, 3, 4$ and their number of orientations m .




























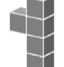







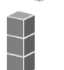





| (x) | m | Shape | (x) | m | Shape |
|------|----|---|------|----|---|
| (M) | 1 |  | (I4) | 3 |  |
| (D) | 3 |  | (L4) | 24 |  |
| (I3) | 3 |  | (O4) | 3 |  |
| (V3) | 12 |  | (P4) | 8 |  |
| (A4) | 12 |  | (S4) | 12 |  |
| (B4) | 12 |  | (T4) | 12 |  |

Table 2
All polycubes (x) of size $n = 5$ and their number of orientations m .

| (x) | m | Shape | (x) | m | Shape | (x) | m | Shape | (x) | m | Shape |
|-------|----|---|-------|----|---|-------|----|---|-------|----|---|
| (A5) | 24 |  | (L25) | 24 |  | (S15) | 24 |  | (V25) | 12 |  |
| (F5) | 24 |  | (L35) | 24 |  | (S25) | 24 |  | (W5) | 12 |  |
| (I5) | 3 |  | (L45) | 24 |  | (T5) | 12 |  | (X5) | 3 |  |
| (J15) | 12 |  | (N5) | 24 |  | (T15) | 12 |  | (Y5) | 24 |  |
| (J25) | 24 |  | (N15) | 24 |  | (T25) | 24 |  | (Z5) | 12 |  |
| (J45) | 24 |  | (N25) | 24 |  | (U5) | 12 |  | | | |
| (L5) | 24 |  | (P5) | 24 |  | (V5) | 12 |  | | | |
| (L15) | 12 |  | (Q5) | 24 |  | (V15) | 12 |  | | | |

polycubes presented in Tables 1 and 2 are shown in Table 3. An overview of all lattice animals of size $n \leq 5$ is given in our previous works [12,13] (see, e.g. large Tables 1 and 2 in [13]). Table 4 shows the number of possible orientations m for polycubes of size $n \leq 6$ and the number of objects $A_3^m(n)$ with the specified number of orientations. Polycubes of size $n \leq 5$ can have 1, 3, 8, 12 or 24 different orientations.

The numerical algorithm used to deposit a lattice animal at randomly chosen places on the 3D substrate was already described in details in the previous papers [12,13]. Therefore, we shall present it briefly, giving the algorithm additions necessary for determining the percolation threshold.

The primary lattice animal is a group of connected sites in the cubic lattice that contains the origin $(0, 0, 0)$. We call that point the head of an object. At each Monte Carlo step, a lattice site is selected randomly. If the chosen site is unoccupied, deposition of the object is tried in one of the 24 orientations, which is chosen randomly. Then, we fix the head of the object at the selected site and search whether all necessary sites are unoccupied. If so, we occupy these sites and place the object. If the attempt fails, a new

Table 3

Several lattice animals (x) of size $n = 5$ and their number of orientations m . All lattice animals of size $n \leq 5$ are displayed in our previous works [12,13].

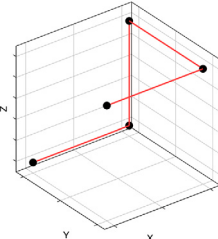
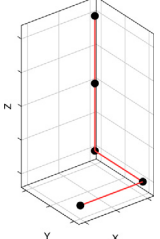
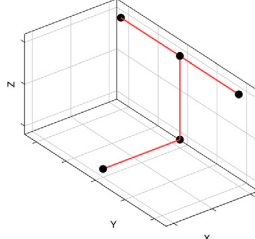
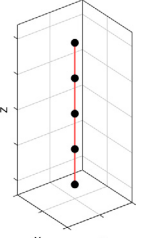
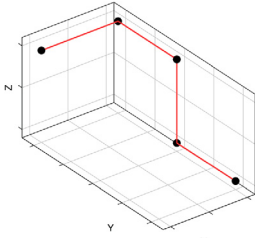
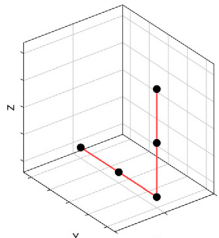
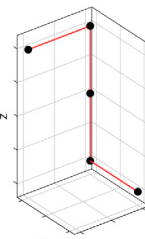
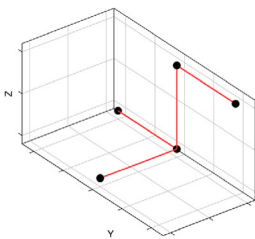
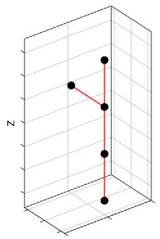
| (x), m | Shape | (x), m | Shape | (x), m | Shape |
|----------|---|----------|---|----------|--|
| (A5),24 |  | (L45),24 |  | (T25),24 |  |
| (I5),3 |  | (N15),24 |  | (V5),12 |  |
| (L15),12 |  | (S25),24 |  | (Y5),24 |  |

Table 4

Shown here is the number of polycubes $A_3^m(n)$ of size n with the specified number of possible orientations $m = 1, 3, 4, 6, 8, 12, 24$. The results are shown for all polycubes of size $n \leq 6$.

| | A_3^1 | A_3^3 | A_3^4 | A_3^6 | A_3^8 | A_3^{12} | A_3^{24} | $N = \sum_m A_3^m$ |
|---------|---------|---------|---------|---------|---------|------------|------------|--------------------|
| $n = 1$ | 1 | | | | | | | 1 |
| $n = 2$ | | 1 | | | | | | 1 |
| $n = 3$ | | 1 | | | | 1 | | 2 |
| $n = 4$ | | 2 | | | 1 | 4 | 1 | 8 |
| $n = 5$ | | 2 | | | | 10 | 17 | 29 |
| $n = 6$ | | 1 | 1 | 3 | | 34 | 127 | 166 |

site and orientation are selected randomly, and so on. The numerical algorithm that searches all possible object orientations and selects the random orientation of a lattice animal is given in the previous paper [12]. We have verified that using different heads for all examined objects gives quantitatively the same results for the temporal evolution of density $\theta(t)$ and the jamming limit θ_j .

The coverage of the surface is increased in the RSA process up to the percolation threshold, when the opposite edges of the system are connected via some path of nearest neighbor sites occupied by the particles. The tree-based union/find algorithm was used to determine the percolation threshold [45,46]. This is the most challenging and time-consuming step of the procedure. Each cluster of connected sites is stored as a separate tree, having a single “root” site. All cluster sites possess pointers to the root site, so it is simple to ascertain whether two sites are members of the same cluster. When a deposited object connects two separate clusters, they are amalgamated by adding a pointer from the root of the smaller cluster to the root of the larger one. This procedure is repeated until the percolation threshold is reached, i.e., until a single cluster connects the opposite sides of the lattice.

The Monte Carlo simulations are performed on a 3D cubic lattice of linear size up to $L_{\max} = 512$. Periodic boundary conditions are used in all directions. The data are averaged over 1024 independent runs for each investigated lattice animal. The time is counted by the number of attempts to select a lattice site and scaled by the total number of lattice sites $L^3 \approx 10\text{--}100$ million.

3. Results

Values of the percolation thresholds for the infinitely large lattice θ_p^* are obtained using the usual finite-size scaling analysis of the percolation behavior on three-dimensional lattices [47]. In such systems one assumes that the effective percolation threshold

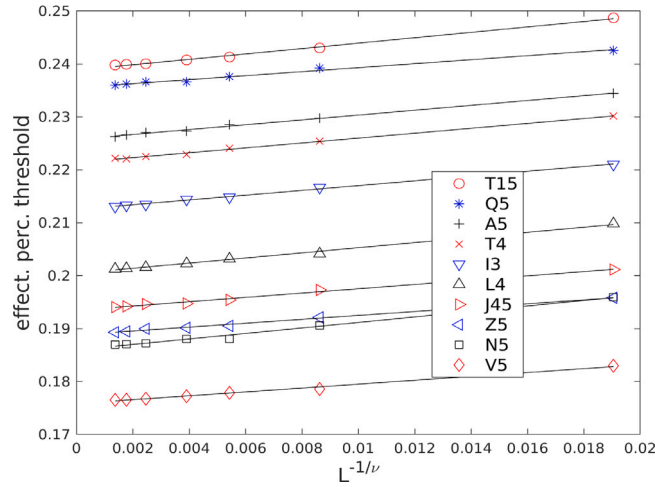


Fig. 1. Finite-size scaling of the percolation threshold θ_p against $L^{-1/\nu}$, with $\nu = 7/8$. The results are given for various lattice animals, as indicated in the legend (see, Tables 1 and 2).

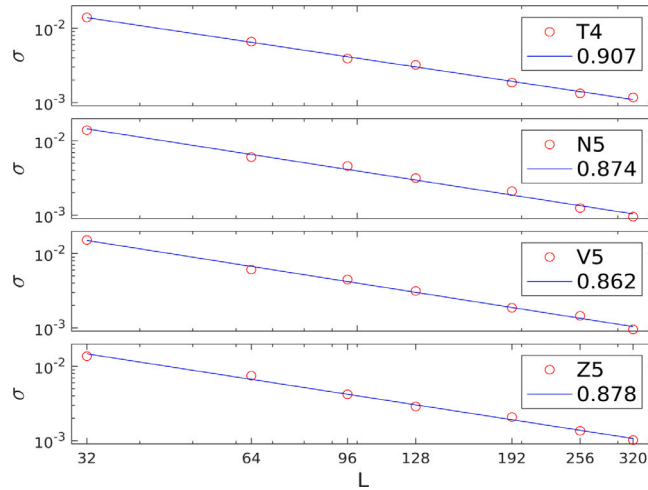


Fig. 2. Standard deviations σ of the percolation threshold on double logarithmic scale for four arbitrarily chosen lattice animals, as indicated in the legend (see, Tables 1 and 2). Straight lines correspond to the best fit according to the power law of Eq. (2) with the values of the exponent ν given on each plot.

$\theta_p(L)$ (the mean value of threshold measured for a finite lattice of linear size L) approaches the asymptotic value $\theta_p(L) \rightarrow \theta_p^*$ for $L \rightarrow \infty$ via the power law:

$$\theta_p(L) - \theta_p^* \propto L^{-1/\nu} . \tag{1}$$

Here the constant ν is the critical exponent that governs the divergence of the correlation length as $\xi \propto |\theta_p - \theta_p^*|^{-\nu}$. It should be noted that the universality class of random percolation in 3D is very well identified and the critical exponents are known, namely, $\nu = 0.8774(13) \approx 7/8$ [48,49]. The latter relationship allows us to extrapolate the threshold for an infinite system, $L \rightarrow \infty$. This kind of behavior, which is expected for systems without long-range correlations, has been observed in previous studies of percolation of extended objects on 3D lattices [40–43,49].

The effective percolation threshold $\theta_p(L)$ for each object was calculated for seven values of the linear lattice size $L = 32, 64, 96, 128, 192, 256, 320$. We plotted the mean value $\theta_p(L)$ of the threshold for various lattice sizes against $L^{-1/\nu}$ which confirmed the validity of the finite-size scaling in the system and enabled us to determine the asymptotic value of the percolation threshold θ_p^* . Finite-size scaling of the lattice threshold $\theta_p(L)$ against $L^{-1/\nu}$ for $\nu = 0.8774(13) \approx 7/8$ [48,49] is illustrated in Fig. 1 for ten arbitrarily chosen lattice animals. Values of the obtained percolation thresholds θ_p^* for all examined objects are given in Tables 5 and 6 together with the corresponding jamming coverages θ_j .

Table 5

For each lattice animal (x) of size $n = 1, 2, 3, 4$ with m possible orientations, $\theta_j^{(x)}$ and $\theta_p^*(x)$ are the jamming coverage and percolation threshold, respectively. Error estimates concerning the last digits are indicated between parentheses. Here, N_1 is the number of first neighbors and R_g is radius of gyration.

| Shape (x), size n | m | N_1 | R_g | $\theta_j^{(x)}$ | $\theta_p^*(x)$ |
|---------------------|-----|-------|--------|------------------|-----------------|
| (M), $n = 1$ | 1 | 6 | 0.0000 | 1.0000(0) | 0.3122(9) |
| (D), $n = 2$ | 3 | 10 | 0.5000 | 0.9184(1) | 0.2566(9) |
| (I3), $n = 3$ | 3 | 14 | 0.8165 | 0.8390(2) | 0.2125(11) |
| (V3), $n = 3$ | 12 | 13 | 0.6667 | 0.8788(2) | 0.2396(10) |
| (A4), $n = 4$ | 12 | 16 | 0.7906 | 0.8178(2) | 0.2260(11) |
| (B4), $n = 4$ | 12 | 16 | 0.7906 | 0.8178(2) | 0.2260(11) |
| (I4), $n = 4$ | 3 | 18 | 1.1180 | 0.7808(3) | 0.1801(11) |
| (L4), $n = 4$ | 24 | 17 | 0.9354 | 0.8339(2) | 0.2004(11) |
| (O4), $n = 4$ | 3 | 16 | 0.7071 | 0.8079(3) | 0.2419(12) |
| (P4), $n = 4$ | 8 | 15 | 0.7500 | 0.7941(3) | 0.2414(12) |
| (S4), $n = 4$ | 12 | 16 | 0.8660 | 0.8149(2) | 0.2206(11) |
| (T4), $n = 4$ | 12 | 16 | 0.8292 | 0.8114(3) | 0.2214(12) |

Table 6

For each lattice animal (x) of size $n = 5$ with m possible orientations, $\theta_j^{(x)}$ and $\theta_p^*(x)$ are the jamming coverage and percolation threshold, respectively. Error estimates concerning the last digits are indicated between parentheses. Here, N_1 is the number of first neighbors and R_g is the radius of gyration.

| Shape (x) | m | N_1 | R_g | $\theta_j^{(x)}$ | $\theta_p^*(x)$ |
|-----------|-----|-------|--------|------------------|-----------------|
| (A5) | 24 | 18 | 0.8485 | 0.7716(2) | 0.2258(11) |
| (F5) | 24 | 19 | 0.9798 | 0.7860(3) | 0.2069(10) |
| (I5) | 3 | 22 | 1.4142 | 0.7369(4) | 0.1555(10) |
| (J15) | 12 | 20 | 1.0583 | 0.7635(2) | 0.1899(11) |
| (J25) | 24 | 19 | 0.9381 | 0.7839(2) | 0.2092(11) |
| (J45) | 24 | 20 | 1.0198 | 0.7958(3) | 0.1934(11) |
| (L5) | 24 | 21 | 1.2329 | 0.7695(3) | 0.1715(11) |
| (L15) | 12 | 20 | 1.0583 | 0.7635(3) | 0.1899(11) |
| (L25) | 24 | 19 | 0.9381 | 0.7839(2) | 0.2092(11) |
| (L35) | 24 | 19 | 0.9798 | 0.7774(3) | 0.2026(11) |
| (L45) | 24 | 20 | 1.0198 | 0.7957(2) | 0.1934(11) |
| (N5) | 24 | 20 | 1.1314 | 0.7866(3) | 0.1860(9) |
| (N15) | 24 | 19 | 0.9798 | 0.7842(2) | 0.2079(13) |
| (N25) | 24 | 18 | 0.8944 | 0.7790(3) | 0.2243(11) |
| (P5) | 24 | 19 | 0.8944 | 0.8017(3) | 0.2201(13) |
| (Q5) | 24 | 18 | 0.8000 | 0.7826(3) | 0.2355(11) |
| (S15) | 24 | 19 | 0.9798 | 0.7841(2) | 0.2079(13) |
| (S25) | 24 | 18 | 0.8944 | 0.7790(3) | 0.2243(11) |
| (T5) | 12 | 20 | 1.0198 | 0.7500(3) | 0.1899(11) |
| (T15) | 12 | 17 | 0.8485 | 0.7582(3) | 0.2388(11) |
| (T25) | 24 | 19 | 0.8944 | 0.7863(2) | 0.2136(12) |
| (U5) | 12 | 20 | 1.0198 | 0.7611(3) | 0.1939(10) |
| (V5) | 12 | 21 | 1.1314 | 0.7628(3) | 0.1758(9) |
| (V15) | 12 | 19 | 0.9381 | 0.7647(3) | 0.2130(11) |
| (V25) | 12 | 19 | 0.9381 | 0.7647(3) | 0.2130(11) |
| (W5) | 12 | 19 | 1.0583 | 0.7615(3) | 0.2033(12) |
| (X5) | 3 | 18 | 0.8944 | 0.7007(3) | 0.2273(12) |
| (Y5) | 24 | 20 | 1.0954 | 0.7595(3) | 0.1877(13) |
| (Z5) | 12 | 20 | 1.0954 | 0.7643(2) | 0.1888(10) |

According to the scaling theory, the standard deviation σ of the percolation threshold measured for a finite lattice L satisfies the power law:

$$\sigma \propto L^{-1/\nu} \tag{2}$$

In Fig. 2 the standard deviation σ vs. L is shown on a double logarithmic scale for several arbitrarily chosen lattice animals. For all lattice animals we confirmed the power law of Eq. (2) with the mean value of the exponent $\nu = 0.882 \pm 0.022$. Therefore, these results are in good agreement with the universal value $\nu \approx 7/8$ [48,49].

Upon examining the percolation threshold values θ_p^* for all objects of size $n \leq 5$ (see, Tables 5 and 6), we concluded that the number of object orientations m is not correlated with the values of θ_p^* . The coverage kinetics is known to be slowed down with the increase in the number of possible placements m of the shape [12]. However, it is not difficult to notice some other geometric properties of the deposited shapes that affect their percolation properties. Each lattice shape is surrounded by the first neighboring sites on the lattice. The obtained results show that the number of an object’s nearest neighbor sites N_1 significantly influences its percolation characteristics. For instance, when considering objects of size $n = 4$, object I4 has the highest number of first neighbors

($N_1 = 18$) and the lowest percolation threshold value ($\theta_p^* = 0.1801(11)$). Object I5, which is a shape of size $n = 5$, has the highest number of first neighbors ($N_1 = 22$) and hence corresponds to the smallest value of the percolation threshold ($\theta_p^* = 0.1555(10)$). Objects L5 and V5 have slightly higher percolation thresholds because they have one less first neighbor than object I5. All other objects of size 5 have fewer first neighbors ($N_1 \leq 20$) and, hence, higher percolation threshold values. Qualitatively, we can say that the value of θ_p^* depends on the object's capability to make connections with other depositing objects. The number of nearest neighbors N_1 seems to be a quantity closely related to the connectivity. Indeed, we observe that the object T15, with the largest threshold ($\theta_p^* = 0.2388(11)$), has the smallest number N_1 of the first neighboring sites on the lattice, i.e. $N_1 = 17$.

From Tables 5 and 6, it can be seen that there are objects of the same size n , with the same number of first neighbors N_1 , whose percolation thresholds θ_p^* differ significantly. The geometric characteristic of the objects that can be related to these changes in the percolation properties of the objects is the radius of gyration R_g . The radius of gyration is defined as the root-mean-square average of the distance of all lattice nodes occupied by the object from the center of mass of the object. Actually, the radius of gyration R_g of a lattice animal of size n that fills the nodes of the grid with coordinates $\{\vec{r}_i\} = \{(x_i, y_i, z_i)\}, i = 1, \dots, n$ is given by the expression

$$R_g = \left[\frac{1}{n} \sum_{i=1}^n s_i^2 \right]^{1/2}, \tag{3}$$

where

$$s_i^2 = (x_i - x_c)^2 + (y_i - y_c)^2 + (z_i - z_c)^2, \tag{4}$$

and

$$x_c = \frac{1}{n} \sum_{i=1}^n x_i, \quad y_c = \frac{1}{n} \sum_{i=1}^n y_i, \quad z_c = \frac{1}{n} \sum_{i=1}^n z_i. \tag{5}$$

For two lattice animals having the same size, the one with the larger radius of gyration is the more extended or less spherical one. If the value of R_g is small, then we can say the object is relatively compact.

In Figs. 3(a) and 4(a), the dependence of the percolation threshold θ_p^* on the radius of gyration R_g is shown for all lattice animals with a size of $n \leq 5$. Figs. 3(b) and 4(b) are included for a simpler insight into the number of nearest neighbors N_1 for each studied object. Due to the greater diversity of lattice animals of size of $n = 5$, let us first analyze the results shown in Fig. 4. It is clear that for lattice animals of the same size, the percolation threshold decreases with an increase in the number of the object's nearest neighbors. Indeed, the values of the percolation threshold θ_p^* for objects with $N_1 = 18$ first neighbors are in the range of $0.223 \lesssim \theta_p^* \lesssim 0.236$. For objects with a greater number of neighbors, the range of the percolation threshold values shifts towards lower values. Thus, for $N_1 = 19$, the percolation threshold is in the range of $0.201 \lesssim \theta_p^* \lesssim 0.221$, for $N_1 = 20$, it is $0.186 \lesssim \theta_p^* \lesssim 0.194$, and for $N_1 = 21$, the range is of $0.170 \lesssim \theta_p^* \lesssim 0.175$. Objects with $N_1 = 17$ and $N_1 = 22$ first neighbors have the highest and lowest percolation threshold values, respectively. Qualitatively the same correlation between the percolation threshold values and the number of first neighbors of objects of size $n < 5$ can be seen in Fig. 3.

If objects of the same size n have the same number of nearest neighbors N_1 , their percolation threshold θ_p^* decreases with an increase in the radius of gyration R_g (see, Figs. 3 and 4). The radius of gyration R_g can be considered as a measure of the compactness of an object. More compact objects have smaller linear dimensions along the lattice directions. For example, objects A5 and I5 are of the same size $n = 5$ (see, Table 3), while their radii of gyration differ significantly. Object I5 is elongated and has a large radius of gyration ($R_g = 1.4142$). Object A5 is compact and rounded, so its radius of gyration is considerably smaller ($R_g = 0.8485$). Compact objects cover space more efficiently and have a lower connecting probability. Compact objects tend to form dense, isolated islands on the lattice. Then, the connectivity in the system is poor at low densities, and percolation sets in at larger density values. This suggests that, for various objects of the same size, the percolation threshold θ_p^* of more compact and rounded shapes (smaller R_g) exceeds the θ_p^* of the elongated ones (larger R_g).

4. Concluding remarks

Our previous work [32] investigated percolation and jamming phenomena for random sequential deposition of objects of various shapes and sizes on a two dimensional (2D) triangular lattice. Self-avoiding lattice steps made the shapes. It has been shown that for various planar objects of the same length, the percolation threshold θ_p^* of more compact shapes (hexagons, triangles) exceeds the θ_p^* of elongated ones (line segments, angled objects). The present study reached similar conclusions by examining a significantly broader class of objects, lattice animals in three dimensions. A systematic approach is made by examining a wide variety of object shapes.

Our results suggest that for lattice animals of the same size:

- (i) the percolation threshold θ_p^* decreases with an increase in the number of the object's nearest neighbors N_1 ;
- (ii) The percolation threshold θ_p^* for compact and rounded objects is higher than for elongated ones. This behavior of the percolation threshold value is consistent with the size of the radius of gyration R_g of the lattice animal. If two objects are of the same size and have the same number of nearest neighbors N_1 , the object with the larger radius of gyration R_g is less compact or more extended. Therefore, as the object's radius of gyration R_g increases, the percolation threshold value θ_p^* decreases.

It is important to emphasize that there are lattice animals of the same size $n = 5$, which have an equal number of nearest neighbors N_1 and the same R_g value, but their percolation thresholds differ slightly (see, Fig. 4). Examples of such shapes are objects P5 and T25, or F5 and L35. We have not been able to identify any other geometric characteristic of the shape that would

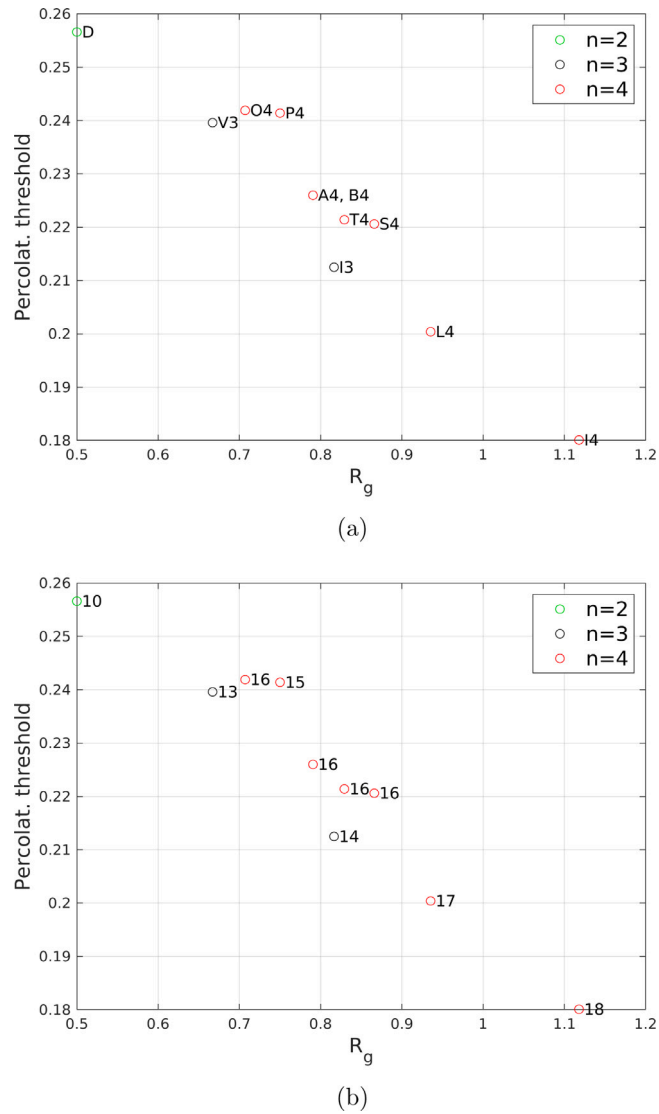
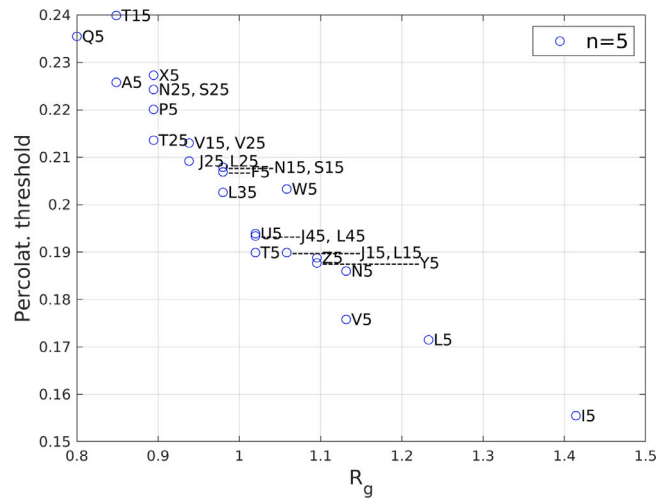


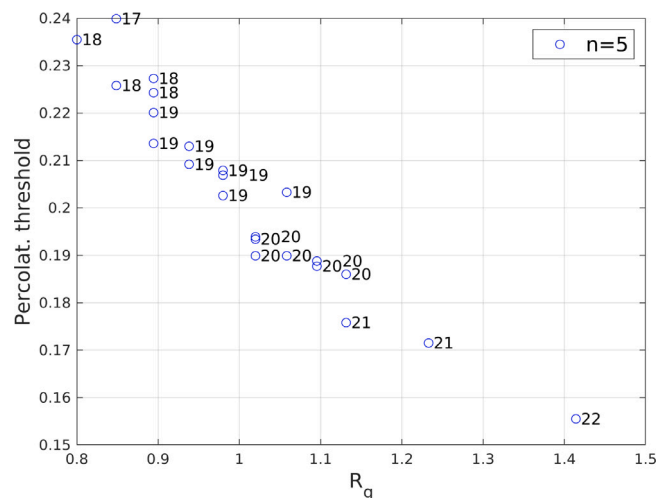
Fig. 3. Dependence of the percolation threshold θ_p^* on the radius of gyration R_g (Eq. (3)) for all lattice animals of size $n = 2, 3, 4$, as indicated in the legend. Both panels display the same results. On the right side of each symbol (circle), the name of the corresponding object (panel (a)) and the number of its first neighbors N_1 (panel (b)) are listed. Next to the symbols corresponding to chiral pairs, the names of both objects are listed. For θ_p^* the error bars do not exceed the size of the symbols.

correlate with this variation in the percolation threshold. In most cases, objects with greater anisotropy have a lower percolation threshold. A more detailed analysis of additional geometric characteristics of the shapes will be the subject of future work.

The model considered here is highly idealized and is not intended to reproduce a particular experimentally studied system. However, this work aims to encourage the development of more advanced models that can reproduce concrete experimental systems. Specifically, percolation theory has been successfully used to study the well-known sol–gel transition [50], in which the percolation threshold determines the point at which a system shifts from a liquid to a gel state. This transition is governed by the ability of molecules to form a network that traps solvent molecules, creating a semi-solid structure. It is well known that the shape of a molecule affects the gelation process by influencing how molecules interact, the number and strength of contact points, their conformational flexibility, and the nature of their self-assembly [51–55]. These factors collectively determine the efficiency and stability of the gel network formed. Examining these points requires a systematic approach using a wide variety of extended objects on a 3D lattice. Accordingly, the percolation of various shapes on 3D lattice could be an interesting topic for further research that will provide a better description of the gelation process.



(a)



(b)

Fig. 4. Dependence of the percolation threshold θ_p^* on the radius of gyration R_g (Eq. (3)) for all lattice animals of size $n = 5$. Both panels display the same results. On the right side of each symbol (circle), the name of the corresponding object (panel (a)) and the number of its first neighbors N_1 (panel (b)) are listed. Next to the symbols corresponding to chiral pairs, the names of both objects are listed. For θ_p^* the error bars do not exceed the size of the symbols.

CRedit authorship contribution statement

D. Stojiljković: Writing – review & editing, Validation, Software, Data curation. **J.R. Šćepanović:** Visualization, Formal analysis. **Z.M. Jakšić:** Writing – review & editing, Validation, Resources, Formal analysis, Data curation. **Lj. Budinski-Petković:** Writing – review & editing, Validation. **S.B. Vrhovac:** Writing – review & editing, Writing – original draft, Visualization, Supervision, Software, Project administration, Methodology, Funding acquisition, Formal analysis, Data curation, Conceptualization.

Declaration of competing interest

The authors declare that they have no known competing financial interests or personal relationships that could have appeared to influence the work reported in this paper.

Acknowledgments

This work was supported by the Ministry of Science, Technological Development and Innovation of the Republic of Serbia. Numerical computations were performed on the PARADOX-IV supercomputing facility at the Scientific Computing Laboratory, National Center of Excellence for the Study of Complex Systems, Institute of Physics Belgrade.

References

- [1] W.F. Lunnon, Counting polyominoes, in: A.O.L. Atkin, B.J. Birch (Eds.), *Computers in Number Theory*, Academic Press, 1971, pp. 347–372.
- [2] D.S. Gaunt, M.F. Sykes, H. Ruskin, Percolation processes in D-dimensions, *J. Phys. A: Math. Gen.* 9 (1976) 1899, <http://dx.doi.org/10.1088/0305-4470/9/11/015>.
- [3] G. Aleksandrowicz, G. Barequet, Counting polycubes without the dimensionality curse, *Discrete Math.* 309 (2009) 4576, <http://dx.doi.org/10.1016/j.disc.2009.02.023>.
- [4] I. Jensen, Enumerations of lattice animals and trees, *J. Stat. Phys.* 102 (2001) 865, <http://dx.doi.org/10.1023/A:1004855020556>.
- [5] D.H. Redelmeier, Counting polyominoes: Yet another attack, *Discrete Math.* 36 (1981) 191, [http://dx.doi.org/10.1016/0012-365X\(81\)90237-5](http://dx.doi.org/10.1016/0012-365X(81)90237-5).
- [6] S. Mertens, M.E. Lautenbacher, Counting lattice animals: A parallel attack, *J. Stat. Phys.* 66 (1992) 669–678, <http://dx.doi.org/10.1007/bf01060088>.
- [7] A.R. Conway, A.J. Guttmann, On two-dimensional percolation, *J. Phys. A: Math. Gen.* 28 (1995) 891, <http://dx.doi.org/10.1088/0305-4470/28/4/015>.
- [8] A.B. Harris, T.C. Lubensky, Connection between percolation and lattice animals, *Phys. Rev. B* 23 (1981) 3591, <http://dx.doi.org/10.1103/PhysRevB.23.3591>.
- [9] M.F. Sykes, M. Glen, Percolation processes in two dimensions. I. Low-density series expansions, *J. Phys. A: Math. Gen.* 9 (1976) 87, <http://dx.doi.org/10.1088/0305-4470/9/1/014>.
- [10] T.C. Lubensky, J. Isaacson, Statistics of lattice animals and dilute branched polymers, *Phys. Rev. A* 20 (1979) 2130, <http://dx.doi.org/10.1103/PhysRevA.20.2130>.
- [11] S. Flesia, D.S. Gaunt, C.E. Soteros, S.G. Whittington, Statistics of collapsing lattice animals, *J. Phys. A: Math. Gen.* 27 (1994) 5831, <http://dx.doi.org/10.1088/0305-4470/27/17/016>.
- [12] I. Lončarević, L. Budinski-Petković, J.R. Šćepanović, Z.M. Jakšić, S.B. Vrhovac, Random sequential adsorption of lattice animals on a three-dimensional cubic lattice, *Phys. Rev. E* 101 (2020) 012119, <http://dx.doi.org/10.1103/PhysRevE.101.012119>.
- [13] M. Beljin-Čavić, I. Lončarević, L. Budinski-Petković, Z.M. Jakšić, S.B. Vrhovac, Simulation study of random sequential deposition of binary mixtures of lattice animals on a three-dimensional cubic lattice, *J. Stat. Mech. Theory Exp.* 2022 (2022) 053206, <http://dx.doi.org/10.1088/1742-5468/ac68dd>.
- [14] J.W. Evans, Random and cooperative sequential adsorption, *Rev. Modern Phys.* 65 (1993) 1281, <http://dx.doi.org/10.1103/RevModPhys.65.1281>.
- [15] S.S. Manna, N.M. Švrakić, Random sequential adsorption: line segments on the square lattice, *J. Phys. A: Math. Gen.* 24 (1991) L671, <http://dx.doi.org/10.1088/0305-4470/24/12/003>.
- [16] J. Talbot, G. Tarjus, P. Van Tassel, P. Viot, From car parking to protein adsorption: an overview of sequential adsorption processes, *Colloids Surf. A* 165 (2000) 287, [http://dx.doi.org/10.1016/S0927-7757\(99\)00409-4](http://dx.doi.org/10.1016/S0927-7757(99)00409-4).
- [17] L. Budinski-Petković, I. Lončarević, D. Dujak, A. Karač, J.R. Šćepanović, Z.M. Jakšić, S.B. Vrhovac, Particle morphology effects in random sequential adsorption, *Phys. Rev. E* 95 (2017) 022114, <http://dx.doi.org/10.1103/PhysRevE.95.022114>.
- [18] M. Sahimi, G. Hunt (Eds.), *Complex media and percolation theory*, in: *Encyclopedia of Complexity and Systems Science Series*, Springer New York, NY, 2021, <http://dx.doi.org/10.1007/978-1-0716-1457-0>.
- [19] M. Sahimi, *Applications of percolation theory*, in: *Applied Mathematical Sciences*, second ed., Springer International Publishing, 2023.
- [20] M.E.J. Newman, D.J. Watts, Scaling and percolation in the small-world network model, *Phys. Rev. E* 60 (1999) 7332, <http://dx.doi.org/10.1103/PhysRevE.60.7332>.
- [21] G. Kondrat, A. Pękalski, Percolation and jamming in random sequential adsorption of linear segments on a square lattice, *Phys. Rev. E* 63 (2001) 051108, <http://dx.doi.org/10.1103/PhysRevE.63.051108>.
- [22] F. Rampf, E.V. Albano, Interplay between jamming and percolation upon random sequential adsorption of competing dimers and monomers, *Phys. Rev. E* 66 (2002) 061106, <http://dx.doi.org/10.1103/PhysRevE.66.061106>.
- [23] G. Kondrat, Influence of temperature on percolation in a simple model of flexible chains adsorption, *J. Chem. Phys.* 117 (2002) 6662, <http://dx.doi.org/10.1063/1.1505866>.
- [24] G. Kondrat, Impact of composition of extended objects on percolation on a lattice, *Phys. Rev. E* 78 (2008) 011101, <http://dx.doi.org/10.1103/PhysRevE.78.011101>.
- [25] J.G. Restrepo, E. Ott, B.R. Hunt, Weighted percolation on directed networks, *Phys. Rev. Lett.* 100 (2008) 058701, <http://dx.doi.org/10.1103/PhysRevLett.100.058701>.
- [26] R.M. Ziff, Explosive growth in biased dynamic percolation on two-dimensional regular lattice networks, *Phys. Rev. Lett.* 103 (2009) 045701, <http://dx.doi.org/10.1103/PhysRevLett.103.045701>.
- [27] N. Tsakiris, M. Maragakis, K. Kosmidis, P. Argyrakis, Percolation of randomly distributed growing clusters: Finite-size scaling and critical exponents for the square lattice, *Phys. Rev. E* 82 (2010) 041108, <http://dx.doi.org/10.1103/PhysRevE.82.041108>.
- [28] A.S. Ioselevich, A.A. Kornyshev, Approximate symmetry laws for percolation in complex systems: Percolation in polydisperse composites, *Phys. Rev. E* 65 (2002) 021301, <http://dx.doi.org/10.1103/PhysRevE.65.021301>.
- [29] N.A.M. Araújo, H.J. Herrmann, Explosive percolation via control of the largest cluster, *Phys. Rev. Lett.* 105 (2010) 035701, <http://dx.doi.org/10.1103/PhysRevLett.105.035701>.
- [30] N.I. Lebovka, N.N. Karmazina, Y.Y. Tarasevich, V.V. Laptev, Random sequential adsorption of partially oriented linear k -mers on a square lattice, *Phys. Rev. E* 84 (2011) 061603, <http://dx.doi.org/10.1103/PhysRevE.84.061603>.
- [31] Y.Y. Tarasevich, N.I. Lebovka, V.V. Laptev, Percolation of linear k -mers on a square lattice: From isotropic through partially ordered to completely aligned states, *Phys. Rev. E* 86 (2012) 061116, <http://dx.doi.org/10.1103/PhysRevE.86.061116>.
- [32] L. Budinski-Petković, I. Lončarević, M. Petković, Z.M. Jakšić, S.B. Vrhovac, Percolation in random sequential adsorption of extended objects on a triangular lattice, *Phys. Rev. E* 85 (2012) 061117, <http://dx.doi.org/10.1103/PhysRevE.85.061117>.
- [33] R. Cohen, K. Erez, D. ben Avraham, S. Havlin, Breakdown of the internet under intentional attack, *Phys. Rev. Lett.* 86 (2001) 3682, <http://dx.doi.org/10.1103/PhysRevLett.86.3682>.
- [34] J. Wang, Z. Zhou, W. Zhang, T.M. Garoni, Y. Deng, Bond and site percolation in three dimensions, *Phys. Rev. E* 87 (2013) 052107, <http://dx.doi.org/10.1103/PhysRevE.87.052107>.
- [35] M.I. González, P.M. Centres, W. Lebrecht, A.J. Ramirez-Pastor, Site-bond percolation on simple cubic lattices: Numerical simulation and analytical approach, *J. Stat. Mech. Theory Exp.* 2016 (2016) 093210, <http://dx.doi.org/10.1088/1742-5468/2016/09/093210>.
- [36] K. Malarz, Simple cubic random-site percolation thresholds for neighborhoods containing fourth-nearest neighbors, *Phys. Rev. E* 91 (2015) 043301, <http://dx.doi.org/10.1103/PhysRevE.91.043301>.
- [37] R.M. Ziff, S. Torquato, Percolation of disordered jammed sphere packings, *J. Phys. A* 50 (2017) 085001, <http://dx.doi.org/10.1088/1751-8121/aa5664>.

- [38] J.-F. Thovert, V.V. Mourzenko, P.M. Adler, Percolation in three-dimensional fracture networks for arbitrary size and shape distributions, *Phys. Rev. E* 95 (2017) 042112, <http://dx.doi.org/10.1103/PhysRevE.95.042112>.
- [39] Y. Tarasevich, V. Cherkasova, Dimer percolation and jamming on simple cubic lattice, *Eur. Phys. J. B* 60 (2007) 97, <http://dx.doi.org/10.1140/epjb/e2007-00321-2>.
- [40] G.D. Garcia, F.O. Sanchez-Varretti, P.M. Centres, A.J. Ramirez-Pastor, Percolation of polyatomic species on a simple cubic lattice, *Eur. Phys. J. B* 86 (2013) 403, <http://dx.doi.org/10.1140/epjb/e2013-40509-1>.
- [41] G. García, F. Sanchez-Varretti, P. Centres, A. Ramirez-Pastor, Random sequential adsorption of straight rigid rods on a simple cubic lattice, *Phys. A* 436 (2015) 558, <http://dx.doi.org/10.1016/j.physa.2015.05.073>.
- [42] P.M. Pasinetti, P.M. Centres, A.J. Ramirez-Pastor, Jamming and percolation of k^2 -mers on simple cubic lattices, *J. Stat. Mech. Theory Exp.* 2019 (2019) 103204, <http://dx.doi.org/10.1088/1742-5468/ab409c>.
- [43] A.C. Buchini Labayen, P.M. Centres, P.M. Pasinetti, A.J. Ramirez-Pastor, Jamming and percolation of k^3 -mers on simple cubic lattices, *Phys. Rev. E* 100 (2019) 022136, <http://dx.doi.org/10.1103/PhysRevE.100.022136>.
- [44] O.F. Inc, Sequence A000162, in: N.J.A. Sloane (Ed.), *The on-Line Encyclopedia of Integer Sequences*, 2019, published electronically.
- [45] M.E.J. Newman, R.M. Ziff, Efficient Monte Carlo algorithm and high-precision results for percolation, *Phys. Rev. Lett.* 85 (2000) 4104, <http://dx.doi.org/10.1103/PhysRevLett.85.4104>.
- [46] M.E.J. Newman, R.M. Ziff, Fast Monte Carlo algorithm for site or bond percolation, *Phys. Rev. E* 64 (2001) 016706, <http://dx.doi.org/10.1103/PhysRevE.64.016706>.
- [47] D. Stauffer, A. Aharony, *Introduction To Percolation Theory*, Taylor & Francis, London, 1994.
- [48] P.H.L. Martins, J.A. Plascak, Percolation on two-and three-dimensional lattices, *Phys. Rev. E* 67 (2003) 046119, <http://dx.doi.org/10.1103/PhysRevE.67.046119>.
- [49] Z. Koza, J. Poła, From discrete to continuous percolation in dimensions 3 to 7, *J. Stat. Mech. Theory Exp.* 2016 (2016) 103206, <http://dx.doi.org/10.1088/1742-5468/2016/10/103206>.
- [50] A. Coniglio, H.E. Stanley, W. Klein, Site-bond correlated-percolation problem: A statistical mechanical model of polymer gelation, *Phys. Rev. Lett.* 42 (1979) 518, <http://dx.doi.org/10.1103/PhysRevLett.42.518>.
- [51] R.B. Jadrich, D.J. Milliron, T.M. Truskett, Colloidal gels, *J. Chem. Phys.* 159 (2023) 090401, <http://dx.doi.org/10.1063/5.0170798>.
- [52] E.J. Garboczi, K.A. Snyder, J.F. Douglas, M.F. Thorpe, Geometrical percolation threshold of overlapping ellipsoids, *Phys. Rev. E* 52 (1995) 819, <http://dx.doi.org/10.1103/PhysRevE.52.819>.
- [53] O. Ursini, R. Angelini, S. Franco, B. Cortese, Understanding the metal free alginate gelation process, *RSC Adv.* 11 (2021) 34449, <http://dx.doi.org/10.1039/D1RA06599H>.
- [54] A. Karoyo, L. Wilson, Physicochemical properties and the gelation process of supramolecular hydrogels: A review, *Gels* 3 (2017) 1, <http://dx.doi.org/10.3390/gels3010001>.
- [55] P. Smerdel, The influence of selected parameters on the size and shape of alginate beads prepared by ionotropic gelation, *Scientia Pharmaceutica* 76 (2008) 77–89, <http://dx.doi.org/10.3797/scipharm.0611-07>.